PAPER • OPEN ACCESS

Effect of parallel flow on resonant layer responses in high beta plasmas

OPEN ACCESS
IOP Publishing | International Atomic Energy Agency
Nuclear Fusion
Nucl. Fusion **64** (2024) 106058 (16pp)
https://doi.org/10.1088/1741-4326/ad703c

Effect of parallel flow on resonant layer responses in high beta plasmas

Yeongsun Lee, Jong-Kyu Park* and Yong-Su Na*

Department of Nuclear Engineering, Seoul National University, Seoul, Korea, Republic Of

E-mail: jkpark@snu.ac.kr and ysna@snu.ac.kr

Received 15 April 2024, revised 21 July 2024
Accepted for publication 16 August 2024
Published 13 September 2024

Abstract

Resonant layers in a tokamak respond to non-axisymmetric magnetic perturbations by amplifying the mode amplitude and balancing the plasma rotation through magnetic reconnection and force balance, respectively. This resonant response can be characterized by local layer parameters and especially by a single quantity in the linear regime, the so-called inner-layer Δ. The computation of Δ under two-fluid drift-MHD formalism has been progressed by reducing the order of the system in the phase space, where the shielding current is approximated as being only carried by electrons, *a posteriori*. In this study, we relax the approximation and compute Δ accounted for by the parallel flow associated with the ion shielding current. The posteriori is numerically verified in great agreement with the original SLAYER developed in a previous paper (J.-K. Park 2022 *Phys. Plasmas* **29** 072506). Extending the resonant layer response theory to high β plasmas, our research findings answer two important questions: how the parallel flow influences the resonant layer response and why the parallel flow effect appears in high β plasmas. The complicated plasma compression in high β regime allows the parallel flow response to give rise to the ion shielding current, which not only shifts the zero-crossing condition of the ExB flow but also enhances the field penetration threshold. Technically, the Riccati matrix transformation method is adapted to handle the numerical stiffness due to the increased order of the system. The high fidelity of this numerical method makes use of further extension of the model to higher-order systems to take other physical phenomena into account. This work is envisaged to predict the resonant layer response under high β fusion reactor conditions.

Keywords: resonant layer response, parallel flow, high beta plasmas

(Some figures may appear in colour only in the online journal)

1. Introduction

The tearing mode [1] is an MHD instability commonly observed in tokamaks. A magnetic perturbation with the wave vector $\vec{k}$ can have a constant phase following the background magnetic field $\vec{B}_0$ nearby a rational surface satisfying the resonant condition $\vec{k}\cdot\vec{B}_0 = 0$, which is often called *the resonant layer*. The resonant layer responds to such a perturbation, typically referred to as *the resonant layer response*, by resonantly growing so that the magnetic configuration is torn by annihilation and reconnection of magnetic fields and consequently equilibrated to an energetically favored state [2]. The resonant layer response is of significance in tokamaks since the plasma performance can be substantially altered due to its consequences due to their resonant nature [3, 4]. It can also be easily triggered by a small external non-axisymmetric field that is always present in reality as well known by the error field problem in tokamaks [5–14]. An important subject in the resonant layer response is how to predict its onset mechanism

* Authors to whom any correspondence should be addressed.

and conditions, which can be parameterized by a single scalar quantity called Δ [1]. This is defined as the discontinuity in the magnetic field normal to the resonant surface, representing the shielding currents within the narrow layer against the magnetic reconnection.

The equilibrium flow can also play a crucial role in the magnetic flux transport through the convection, making the resonant layer response highly selective to the natural flow frequency. For instance, it is believed that the magnetic topology is always equilibrated to a fully-reconnected state, *the mode penetration*, in the absence of plasma rotation, because the magnetic flux diffuses out and the associated shielding current vanishes resulting in $\Delta \to 0$ [3, 4]. Conversely, the mode is stabilized, i.e. the resonant amplification of the perturbed magnetic flux is hindered, if the mode rotates in the rest frame of plasmas (or electrons in the two-fluid description). The mechanism is that the magnetic convection by the plasma rotation circulates the magnetic flux diffused by a finite resistivity [15], maintaining the magnetic equilibrium with the shielding currents. As will be suggested by the results of this work, the magnetic equilibrium can be sustained by the perturbed flow even in the absence of the equilibrium flow.

The resonant layer response theories [16–19] include complex physics such as $E \times B$ and diamagnetic flow effect, finite Larmor radius effect, and collisionless effects through the two-fluid drift-MHD model [20–22] to take into account the slow varying time scales and the comparableness of the order of diamagnetic flow and $E \times B$ flow. Meanwhile, the perturbed parallel flow (response of the parallel flow and referred to hereafter as 'parallel flow' for brevity), which is different from the equilibrium parallel flow [23–30], has been neglected by limiting an interest in low *toroidal* β plasmas, to our knowledge [15–17, 19, 31]. Under this approximation, the mode ends up being locked to the electron rotation through the mode penetration. This is *the electron rotation resonance*. Even though the numerical studies [18, 32, 33] have extended the capability of predicting the experimental threshold [6–8, 10, 13, 34–37] possessed by theory [15–17, 19, 31] to analytically intractable regimes, the zero-crossing property of Δ remains unchanged across the electron rotation resonance. However, a question arises: is it impossible for the shielding current to exist, i.e. $|\Delta| > 0$, at the electron flow resonant condition? Indeed, it was reported in TEXTOR experiments that the minimum value of the field penetration threshold is non-zero and the corresponding rotation is even shifted toward the ion rotation direction [38, 39], suggesting the possibility of a non-zero shielding current. The current carried by ions would be essential for interpreting the observations that have been missed in the models as neglecting the parallel flow. In addition, the neglect is inappropriate for high β plasmas. The parallel flow should be evidently considered for not only ensuring an engineering margin for designing the future machine [9, 40–42] with better confidence but also exploring the fidelity of the fusion reactor regime.

The resonant layer response theory often adopted the boundary layer method [43]. The layer equations are separately solved in the inner and outer layers, and subsequently the solutions are matched. The parallel flow complicates the computation of the inner layer $\Delta_{\rm in}$ by increasing the order of the system. A numerical computation is a preferable alternative for accurate $\Delta_{\rm in}$ provided that the system is analytically intractable in the inner layer. In fact, the fidelity of the Riccati transformation method to handle numerical stiffness was demonstrated by SLAYER in [18]. However, the improved Riccati transformation method should be applied for solving the full layer equations due to the higher-order differential equations of the system. To make use of asymptotically imposed boundary conditions, we adapt the method to the case of two-point boundary conditions [44, 45]. Thereafter, the resonant layer response is explored with the help of the quasi-linear analysis and Δ accounted by the parallel flow. The proposed method extends SLAYER into high β plasmas that is a subroutine to compute the correct $\Delta_{\rm in}$ in GPEC [46]. This study is envisaged to design the error field correction and to predict the field penetration in future fusion reactors [47–50].

This paper is organized as follows. In section 2, we review layer physics models such as the physical meaning of the parallel flow, the relation between the parallel flow and compressibility and boundary conditions. In section 3, the Riccati transformation method is adapted to consider asymptotic boundary conditions and applied to our problem by imposing the associated boundary conditions. Then, the effect of parallel ion flow is elucidated in section 4.

2. Layer physics

For clarity in this paper, we present a complete description of the layer physics. Assuming that the resonant perturbations do not modify the magnetic equilibrium, we set the Taylor problem [3, 4]. Thus, the outer layer solution is analytically tractable in both slab [4, 16] and cylindrical [17, 31] geometries. More practically, it can be solved using the proper numerical tool like IPEC [32]. To manifestly present the parallel flow effect, we shall simplify the geometry and ignore the toroidal mode coupling effect [51–55].

In this work, the tokamak geometry is approximated as a sheared-slab Cartesian with a coordinate (x, y, z) and unit basis vectors $(\hat{x}, \hat{y}, \hat{z})$ characterized by $\vec{B}_0$:

$$\vec{B}_0 = x\hat{y} + B_0\hat{z}, \tag{1}$$

normalized to $B_{\rm a}$ (with the relevant magnitude of the *poloidal* magnetic field). The slab approximation is not merely used to simply present the parallel flow effect in a complete form. In fact, the approximation is reasonable because the inner layer is localized at the rational surface compared to the outer region and thin enough to ignore curvature effects. The origin is laid on the radial position of the rational surface r_s with safety factor $q = m/n$, the poloidal mode number m and the toroidal mode number n. $x = (r - r_{\rm s})/a$, $y = (m\theta - n\phi_{\rm g})/ak$ and $z \approx R_0\phi_{\rm g}/a$ with the radial position r, the scale length a, the poloidal angle θ, the toroidal angle $\phi_{\rm g}$, $k = |\vec{k}|$ and the major radius R_0. The system is invariant and periodic along $\hat{z}$ and $\hat{y}$, respectively. Then, perturbations have the form of $\tilde{A}(x, y, z, t) = \tilde{A}(x, t)\exp(iky)$.

We adopt the two-fluid drift-MHD formulation by Fitzpatrick and Waelbroeck [22] (originated from the original four-field model of Hazeltine and Meiss [20]) constituting the generalized Ohm's law, ion momentum equation and energy equation,

$$\vec{E}+\vec{V}\times\vec{B}+d_{\rm i}\left(\vec{\nabla}P-\frac{\tau}{1+\tau}\left(\vec{b}\cdot\vec{\nabla}P\right)\vec{b}-\vec{J}\times\vec{B}\right)=\eta\vec{J}, \tag{2}$$

$$\left[\left(\partial_t+\vec{V}\cdot\vec{\nabla}+\frac{\tau}{1+\tau}\vec{V}_*\cdot\vec{\nabla}\right)\vec{V}-\frac{\tau}{1+\tau}\vec{V}_*\cdot\vec{\nabla}\left(\left[\vec{b}\cdot\vec{V}\right]\vec{b}\right)\right] =\vec{J}\times\vec{B}-\vec{\nabla}P+\mu_i\vec{\nabla}^2\vec{V}_{\rm i}, \tag{3}$$

$$\left(\partial_t+\vec{V}\cdot\vec{\nabla}\right)P=-\Gamma P\vec{\nabla}\cdot\vec{V}, \tag{4}$$

where $\vec{E}$ is the electric field (normalized to $B_{\rm a}V_{\rm a}$ with the Alfvénic velocity $V_{\rm a}=B_{\rm a}/\sqrt{\mu_0 n_0 m_{\rm i}}$ of $B_{\rm a}$), $\vec{B}$ is the magnetic field (normalized to $B_{\rm a}$), $\vec{J}$ is the current density (normalized to $B_{\rm a}/\mu_0 a$), $\vec{V}$ is the plasma guiding-center velocity (normalized to $V_{\rm a}$), P is the total pressure (normalized to $B_{\rm a}^2/\mu_0$), η is the plasma resistivity (normalized to $\mu_0 V_{\rm a} a$), $\mu_{\rm i}$ is the ion viscosity (normalized to $n_0 m_{\rm i} V_{\rm a} a$), $\Gamma=5/3$ is the plasma ratio of specific heats and $d_{\rm i}=\sqrt{m_{\rm i}/n_0 e^2\mu_0}/a$ is the normalized ion skin-depth. $\vec{V}_*=\vec{b}\times\vec{\nabla}P/en_0B$ is the diamagnetic flow velocity (normalized to $V_{\rm a}$) and $\vec{V}_{\rm i}=\vec{V}+[\tau/(1+\tau)]\vec{V}_*$ is the ion velocity (normalized to $V_{\rm a}$), where $\vec{b}=\vec{B}/|\vec{B}|$ and $\vec{\tau}=T_{\rm i}/T_{\rm e}$ with the electron and ion temperature $T_{\rm e,i}$, respectively.

Equations (2)–(4) neglected the thermal conductivity and electron viscosity. Although a recent paper [17] shed light on the importance of anomalous perpendicular diffusion, to present a parallel flow role simply, we shall nevertheless neglect them in order to focus on the parallel flow effect.

$\vec{B}$ and $\vec{V}$ can be represented by four fields (ψ, ϕ, b_z and V_z),

$$\vec{B}=\vec{\nabla}\psi\times\hat{z}+(B_0+b_z)\hat{z}, \tag{5}$$

$$\vec{V}=\vec{\nabla}\phi\times\hat{z}+V_z\hat{z}. \tag{6}$$

We radially symmetrize the system based on the outward direction for simplicity and then impose the boundary condition $\psi(\pm1,y,t)=-1/2+\Xi(t)\exp(iky)$, where $\Xi(t)$ is the perturbed magnetic flux at the edge determined by the quasi-static external resonant field, $|{\rm d}\ln(\Xi)/{\rm d}t|\ll0$, e.g. the error field.

At the outer region ($x\neq0$), take $\hat{z}\cdot\vec{\nabla}\times$ on equation (3) and then the lowest order of the outcome is $[\vec{\nabla}\psi,\psi]\approx -ikx({\rm d}^2\tilde{\psi}/{\rm d}x^2-k^2\tilde{\psi})=0$ where $[A,B]=\hat{z}\cdot\vec{\nabla}A\times\vec{\nabla}B$. Except for the singular point $x=0$, ${\rm d}^2\tilde{\psi}/{\rm d}x^2-k^2\tilde{\psi}=0$ is satisfied. We decompose the solution using $\tilde{\psi}=\tilde{\psi}_s+\tilde{\psi}_w$, where $\tilde{\psi}_s(x,y,t)=\Psi(t)\hat{\psi}_s(x)\exp(iky)$ and $\tilde{\psi}_w(x,y,t)=\Xi(t)\hat{\psi}_w(x)\exp(iky)$ with the separate boundary conditions $\hat{\psi}_s(0,t)=1$, $\hat{\psi}_s(\pm1,t)=0$, $\hat{\psi}_w(0,t)=0$ and $\hat{\psi}_s(\pm,t)=1$. The exact solution is

$$\tilde{\psi}_s(x,y,t)=\Psi(t)\left(\cosh kx-\frac{\sinh k|x|}{\tanh k}\right)\exp(iky), \tag{7}$$

$$\tilde{\psi}_w(x,y,t)=\Xi(t)\frac{\sinh k|x|}{\sinh k}\exp(iky). \tag{8}$$

The relation of Ψ to Δ is found by the asymptotic matching. The jump condition, $\Delta\tilde{\psi}=[\partial_x\tilde{\psi}]_{0^-}^{0^+}$, gives,

$$\Psi(t)=\frac{\Delta_{sw}\Xi(t)}{\Delta-\Delta_{ss}} \tag{9}$$

where $\Delta_{ss}=-2k/\tanh k$ is the classical tearing index ($\Delta\Psi=\Delta_{ss}\Psi$ with $\Xi=0$) and $\Delta_{sw}=2k/\sinh k$ is a measure of the free energy source provided by the externally resonant field.

Suppose the 'no slip' constraint [31, 56, 57] due to the quasi-static assumption of Ξ and exclude the possibility of rotating boundary perturbation [58]. Impose the plasma rotation boundary condition $V(\pm1,t)=V_0$. Taking a flux-averaging $<\ldots>=\frac{k}{2\pi}\int_0^{2\pi/k}\ldots{\rm d}y$ on y-component of equation (3), and then the equation for velocity is

$$\frac{\partial V(x,t)}{\partial t}=-\frac{k}{2}|\Psi|^2\Im(\Delta)\,\delta(x)+\mu_{\rm i}\frac{\partial^2V}{\partial x^2} \tag{10}$$

where the first term on the RHS is the magnetic braking force obtained from $<\vec{J}\times\vec{B}\cdot\hat{y}>$ using $<\Re(\tilde{f})\Re(\tilde{g})>=\frac{1}{2}\Re(fg^*)$. The second term is the viscous force. If the magnetic braking force is compensatable by the restoring viscous force, the exact solution of equation (10) under the equilibrium with the no-slip constraint is

$$V(x)=V_0-\frac{k}{2\mu_i}|\Psi|^2\Im(\Delta)(1-|x|). \tag{11}$$

Similarly, the equilibrium parallel flow can be given by following the same procedure on the z-component of equation (10). Nonetheless, we simplify the equilibrium parallel flow as a constant to focus on the parallel flow response in the absence of equilibrium flow shear.

Being independent of the inner layer analysis, the outer layer analysis can be improved by IPEC [32].

To find Δ, the singularity in the inner region ($x\approx0$) should be resolved by considering higher-order terms. By taking $\hat{z}\cdot$ and $\hat{z}\cdot\vec{\nabla}\times$ on equation (2), it reduces to

$$[\psi,\phi]=\frac{d_{\rm i}}{1+\tau}[b_z,\psi]+\eta\vec{\nabla}^2\psi \tag{12}$$

and

$$[b_z,\phi]=\left[V_z+d_{\rm i}\vec{\nabla}^2\psi,\psi\right]-B_0\left(\vec{\nabla}\cdot\vec{V}\right)+\eta\vec{\nabla}^2b_z \tag{13}$$

where $(\vec{\nabla}\cdot\vec{V})\sim O(1/B_0)$ represents the almost incompressible condition. By taking $\hat{z}\cdot$ and $\hat{z}\cdot\vec{\nabla}\times$ on equation (3), it reduces to

$$[V_z,\phi]=[b_z,\psi]+\mu_{\rm i}\vec{\nabla}^2V_z \tag{14}$$

and

$$[U,\phi] = -\frac{d_\mathrm{i}}{2}\frac{\tau}{1+\tau}\left(\vec{\nabla}^2[\phi,b_z] + [U,b_z] + \left[\vec{\nabla}^2 b_z,\phi\right]\right) + \left[\vec{\nabla}^2\psi,\psi\right] + \mu_\mathrm{i}\vec{\nabla}^2\left(U + \frac{d_\mathrm{i}\tau}{1+\tau}\vec{\nabla}^2 b_z\right) \quad (15)$$

where $U = -\vec{\nabla}\times\vec{V}\cdot\hat{z}$. By taking the lowest order of equation (4), it reduces to

$$[b_z,\phi] = \frac{\Gamma P_0}{B_0}\left(\vec{\nabla}\cdot\vec{V}\right). \quad (16)$$

Previous study has neglected $[V_z,\psi]$ as *a posteriori*. This approximation is useful to mathematically close equations (12), (13), (15) and (16) with three unknown fields (ψ, ϕ and b_z) after eliminating $(\vec{\nabla}\cdot\vec{V})$. However, it should be recognized that this treatment is physically equivalent to ignoring the ion shielding current. The term $[V_z,\psi]$ in equation (13) originates from the reduction of equation (2), i.e. $\hat{z}\cdot\vec{\nabla}\times[(V_z\,\hat{z})\times\vec{B}] = [V_z,\psi]$. It follows that $V_z \approx V_{\mathrm{i}z}$ due to negligible V_{*z}. Therefore, the posterior forces the current only to be carried by electrons, i.e. $d_\mathrm{i}J_z = V_{\mathrm{i}z} - V_{\mathrm{e}z} \approx -V_{ez}$. To incorporate the ion shielding effect into Δ, it is essential to retain $[V_z,\psi]$ given that $\Delta = [\partial_x\psi]_{0^-}^{0^+}/\psi = -\int_{0^-}^{0^+} J_z\mathrm{d}x/\psi$.

Normalize and linearize equations (12)–(16) and eliminate $\vec{\nabla}\cdot\vec{V}$. The final equations become

$$i(Q-Q_{*\mathrm{e}})\tilde{\psi} = iX\left(\tilde{\phi}-\tilde{Z}\right) + \frac{\mathrm{d}^2\tilde{\psi}}{\mathrm{d}X^2} + O\left(\varepsilon^2\right), \quad (17)$$

$$iQ\tilde{Z} = iQ_{*\mathrm{e}}\tilde{\phi} + iD^2X\frac{\mathrm{d}^2\tilde{\psi}}{\mathrm{d}X^2} + ic_\beta^2 X\tilde{V}_z + c_\beta^2\frac{\mathrm{d}^2\tilde{Z}}{\mathrm{d}X^2} + O\left(\varepsilon^2\right), \quad (18)$$

$$i(Q-Q_{*\mathrm{i}})\frac{\mathrm{d}^2\tilde{\phi}}{\mathrm{d}X^2} = iX\frac{\mathrm{d}^2\tilde{\psi}}{\mathrm{d}X^2} + P\frac{\mathrm{d}^4\left(\tilde{\phi}+\tau\tilde{Z}\right)}{\mathrm{d}X^4} + O\left(\varepsilon^2\right), \quad (19)$$

$$iQ\tilde{V}_z = -iQ_{*\mathrm{e}}\tilde{\psi} + iX\tilde{Z} + P\frac{\mathrm{d}^2\tilde{V}_z}{\mathrm{d}X^2} + O\left(\varepsilon^2\right), \quad (20)$$

where $Z = b_z d_\mathrm{i}/(1+\tau)$, $\bar{V}_z = V_z d_\mathrm{i}/(1+\tau)$, of which bar is neglected in the above final equations, $c_\beta = \sqrt{\beta/(1+\beta)}$ with $\beta = \Gamma P_0/B_0^2$ and $P = \mu_\mathrm{i}/\eta$. The background equilibrium is given by $\psi_0(x) = -x^2/2$, $\phi_0(x) = -Vx$, $Z_0(x) = V_{\mathrm{e}*}x$, and $V_{z0} = 0$, where $V = V_{y0}(x=0)$ and $V_{\mathrm{e}*}$ is the electron diamagnetic velocity. The other parameters are normalized and the variable x is stretched using a small parameter $\varepsilon = (\eta/k)^{1/3}$: $Q = V/\varepsilon$, $Q_{*\mathrm{e}} = -V_{*\mathrm{e}}/\varepsilon$, $Q_{*\mathrm{i}} = -V_{*\mathrm{i}}/\varepsilon$, $D = c_\beta d_\mathrm{i}/\varepsilon\sqrt{1+\tau}$ and $X = x/\varepsilon$.

The shielding current vanishes under the electron rotation resonance ($Q = Q_{*\mathrm{e}}$) in low β limit ($c_\beta \to 0$). This is clarified by equating equations (17) and (18),

$$\frac{\mathrm{d}^2\tilde{\psi}}{\mathrm{d}X^2} = 0 \text{ if } Q = Q_{*\mathrm{e}} \text{ and } c_\beta = 0. \quad (21)$$

Meanwhile, the parallel flow contributes Δ_in as β increases. To gain some understanding of the mechanics between the parallel flow and compressibility, rearrange equation (18) as

$$\left(iQ_{*\mathrm{e}}\tilde{\phi} - iQ\tilde{Z}\right) + \frac{1}{\beta}\left(iQ_{*\mathrm{e}}\tilde{\phi} - iQ\tilde{Z}\right) + \frac{iD^2X}{c_\beta^2}\frac{\mathrm{d}^2\tilde{\psi}}{\mathrm{d}X^2} + iX\tilde{V}_z + \frac{\mathrm{d}^2\tilde{Z}}{\mathrm{d}X^2} = 0. \quad (22)$$

The second term corresponds to $B_0(\vec{\nabla}\cdot\vec{V})$ and the fourth term does to $[V_z,\psi]$ in equation (13). In low β plasmas, plasmas are easy to compress and the ordering $(iQ_{*\mathrm{e}}\tilde{\phi} - iQ\tilde{Z}) \sim O(\beta)$ is roughly satisfied. Then, under electron rotation resonance, not only the equilibrium electron flow $(Q - Q_{*\mathrm{e}})$ but also the perturbed electron flow $(\tilde{\phi} - \tilde{Z})$ do annihilate in equation (17), leading to $\mathrm{d}^2\tilde{\psi}/\mathrm{d}X^2 \approx 0$. However, as β increases, plasma compression becomes more difficult and the gap between $\tilde{\phi}$ and $\tilde{Z}$ gives rise to a room for the parallel flow to play a role in equation (22). For further high β such as in the $\beta \to \infty$ limit, the terms including $(\tilde{\phi} - \tilde{Z})$ become subdominant. This will be further elucidated quantitatively in section 4 through solution reconstruction.

We decompose Δ_in with the help of equation (18) for clear interpretation of which species carry the shielding current,

$$\Delta_\mathrm{in} = \Delta_\mathrm{in}^\mathrm{ion} + \Delta_\mathrm{in}^\mathrm{electron}, \quad (23)$$

where $\Delta_\mathrm{in}^\mathrm{ion} = -\frac{1}{\Psi}\int_\infty^\infty \mathrm{d}X\frac{c_\beta^2}{D^2}\tilde{V}_z$ and $\Delta_\mathrm{in}^\mathrm{electron} = \frac{1}{\Psi}\int_\infty^\infty \mathrm{d}X\left[\frac{Q\tilde{Z}-Q_{*\mathrm{e}}\tilde{\phi}}{D^2X} + \frac{ic_\beta^2}{D^2X}\frac{\mathrm{d}^2\tilde{Z}}{\mathrm{d}X^2}\right]$. The decomposition will be used in section 4 to demonstrate that the shielding current nearby $Q \sim Q_{*\mathrm{e}}$ is carried by ions.

$\tilde{\psi}$ has a tearing parity (even). Substituting $\tilde{\psi}$ into equations (17)–(20) reveals $\tilde{\phi}, \tilde{Z}$ has odd parities and $\tilde{V}_z$ has an even parity.

$$\tilde{\psi}(X) = \tilde{\psi}(-X) \quad (24)$$

$$\tilde{\phi}(X) = -\tilde{\phi}(-X) \quad (25)$$

$$\tilde{Z}(X) = -\tilde{Z}(-X) \quad (26)$$

$$\tilde{V}_z(X) = \tilde{V}_z(-X). \quad (27)$$

The asymptotic matching condition of Δ to the outer region demands annihilation of the higher-order power term $|X|^n$, $n \geqslant 2$, at the large X limit. These conditions enforce $\tilde{\psi}$ to have the below asymptotic behavior,

$$\tilde{\psi}(X) \to \Psi\left[1 + \frac{\Delta_\mathrm{in}}{2}|X| + O\left(\frac{1}{X}\right)\right] \quad (28)$$

where $\Delta_\mathrm{in} = \varepsilon\Delta$

By taking one-side asymptotic expansion in the large X limit $\tilde{A} \to \sum_l \tilde{A}_l|X|^l$, where $\tilde{A}_l$ is a coefficient of power, l is an

integer and $\tilde{A}$ can be $\tilde{\phi}$, $\tilde{Z}$ and $\tilde{V}_z$, where asymptotic behavior of four fields is fully obtained,

$$\tilde{\phi} \to Q\Psi\frac{1}{X}\left(1+|X|\frac{\Delta_{\text{in}}}{2}+O\left(\frac{1}{|X|}\right)\right), \tag{29}$$

$$\tilde{Z} \to Q_{*e}\Psi\frac{1}{X}\left(1+|X|\frac{\Delta_{\text{in}}}{2}+O\left(\frac{1}{|X|}\right)\right), \tag{30}$$

$$\tilde{V}_z \to O\left(\frac{1}{|X|^3}\right). \tag{31}$$

Δ can be obtained by solving equations (17)–(20) with the boundary conditions, equations (24)–(31):

$$\Delta = \frac{\Delta_{\text{in}}\left(Q, Q_{*\text{i}}, Q_{*\text{e}}, c_\beta, D, P\right)}{\varepsilon}. \tag{32}$$

Solving equations (17)–(20) is analytically intractable due to retained $\tilde{V}_z$. As a reliable alternative, we employ the numerical calculation in section 3.

Rewrite equation (11) as

$$\Xi^2 = 2\varepsilon^4 P\frac{|\Delta(Q)-\Delta_{ss}|^2}{|\Delta_{sw}|^2\Im(\Delta(Q))}(Q_0-Q) \equiv f(Q), \tag{33}$$

with $Q_0 = V_0/\varepsilon$ and then, equations (32) and (33) close the problem and make it complete.

Amplitude of Ψ (given by equation (9)) and the solution existence of equation (33) quantitatively indicate how the layer responds to the resonant perturbations. In the presence of the shielding current $|\Delta| \sim |O(1/\varepsilon)| \gg |\Delta_{ss}|$, the singular behavior of equation (33) is resolved using $|\Delta(Q)-\Delta_{ss}|^2 \approx |\Delta(Q)|^2 - 2\Re(\Delta)\Delta_{ss}$. The approximated form of equation (33) is

$$\Xi^2 \approx 2\varepsilon^4 P\frac{|\Delta|-2\cos(\phi_\Delta)\Delta_{ss}}{|\Delta_{sw}|^2\sin(\phi_\Delta)}(Q_0-Q) \equiv f'(Q), \tag{34}$$

where $\phi_\Delta = \tan^{-1}(\frac{\Im(\Delta)}{\Re(\Delta)})$. The equilibrium Q exists if $\Xi^2 \leqslant \max(f')$. In such a case, the mode is stabilized and thus the resulting Ψ is

$$|\Psi(t)| \ll |\Psi_c(t)|, \quad \text{if } |\Delta| \gg 0, \tag{35}$$

where $\Psi_c(t)$ is an amount of the fully-reconnected flux in the absence of the shielding current ($\Delta = 0$) [3, 4, 15],

$$\Psi_c(t) = \frac{\Delta_{sw}\Xi(t)}{-\Delta_{ss}}. \tag{36}$$

The small island size $\sim\sqrt{\Psi(t)}$ justifies the quasi-linear analysis of the force balance. However, the mode stabilization cannot be sustained for high Ξ^2 exceeding $\Xi^2_{\text{crit}} \equiv \max(f')$,

$$\Xi^2_{\text{crit}} = \max\left[2\varepsilon^4 P\frac{|\Delta|-2\cos(\phi_\Delta)\Delta_{ss}}{|\Delta_{sw}|^2\sin(\phi_\Delta)}(Q_0-Q)\right]. \tag{37}$$

Then, Q goes to a value satisfying $(\Xi^2 - f(Q-0))\cdot(\Xi^2 - f(Q+0)) < 0$, the associated Δ goes to 0 and the resulting Ψ rapidly grows. This is the mode penetration. After the mode penetration, the nonlinear framework should be considered. The presented interpretation only suggests an onset of mode penetration.

3. Riccati transformation method to solve the boundary layer problem

The Riccati transformation method for linear two-point boundary value problems was well organized in [44, 45]. However, the boundary conditions, i.e. equations (28)–(31), are asymptotically given. It is complicated to determine the large X required for imposing the boundary conditions. Therefore, it is still worth reviewing how the Riccati transformation method works and subsequently applying this method to the boundary layer problem.

The heuristic understanding of the Riccati transformation is based on how we can extract physical solutions from fundamental solutions by decoupling them. Let us suppose that a target system to solve has a form $Y' = AY$, where the prime denotes a spatial derivative and $Y = [y1, y2]^T$, with $Y' \in \mathbf{C}^n$, $Y \in \mathbf{C}^n$, $A \in \mathbf{C}^{n\times n}$, $y_1 \in \mathbf{C}^q$, $y_2 \in \mathbf{C}^p$ and $p+q=n$,

$$\frac{\mathrm{d}}{\mathrm{d}X}\begin{bmatrix}y_1\\y_2\end{bmatrix} = \begin{bmatrix}A_{11} & A_{12}\\A_{21} & A_{22}\end{bmatrix}\begin{bmatrix}y_1\\y_2\end{bmatrix}. \tag{38}$$

Here, $A = [[A_{11}\ A_{12}]\ [A_{21}\ A_{22}]]$ with $A_{11} \in \mathbf{C}^{q,q}$, $A_{12} \in \mathbf{C}^{q,p}$, $A_{21} \in \mathbf{C}^{p,q}$ and $A_{22} \in \mathbf{C}^{p,p}$.

We transform Y to $W = [w_1, w_2]^T$ with $W \in \mathbf{C}^n$, $w_1 \in \mathbf{C}^q$ and $W_2 \in \mathbf{C}^p$ by taking the inverse of the lower block triangular matrix $T \in \mathbf{C}^{n,n}$,

$$\begin{bmatrix}w_1\\w_2\end{bmatrix} = T^{-1}\begin{bmatrix}y_1\\y_2\end{bmatrix}, \quad T = \begin{bmatrix}I_q & 0\\R & I_p\end{bmatrix}. \tag{39}$$

where I_p and I_q are the identity matrix with rank p and q, respectively. $R \in \mathbf{C}^{p,q}$ is the Riccati matrix.

If the matrix $U = [[U_{11}\ U_{12}]\ [U_{21}\ U_{22}]]$ in the ODE system $W' = UW$ is an upper triangular block matrix, the derivative of w_2 is decoupled from that of w_1,

$$\frac{\mathrm{d}}{\mathrm{d}X}\begin{bmatrix}w_1\\w_2\end{bmatrix} = \begin{bmatrix}U_{11} & U_{12}\\0 & U_{22}\end{bmatrix}\begin{bmatrix}w_1\\w_2\end{bmatrix}, \tag{40}$$

where $U \in \mathbf{C}^{n,n}$, $U_{11} \in \mathbf{C}^{q,q}$, $U_{12} \in \mathbf{C}^{q,p}$, $U_{21} \in \mathbf{C}^{p,q}$, $U_{22} \in \mathbf{C}^{p,p}$ and elements of U_{21} are 0. The merit of this representation is that we can reduce the number of fundamental solutions including fast growing and decaying ones. For instance, the condition $w_2(X) = 0$ can be always satisfied if $w_2(0) = 0$ with the forward integration. Then, the number of fundamental solutions decrease by p. Once y_2 and R are initialized to be the zero vector and matrix, respectively, the initial condition of w_2 is also the zero vector due to $Rw_1 + w_2 = y_2$ from equation (39). Taking this benefit, the parity boundary conditions suggest that $y_{2,i} = \tilde{A}_{\text{odd},i}$ with $i \in \{1,\ldots p\}$ where $\tilde{A}_{\text{odd},i}$ is ith perturbed fields with odd parity to set $y_2(0) = 0$.

The transformation from equations (38)–(40) demands

$$\frac{\mathrm{d}}{\mathrm{d}X}T = AT - TU, \tag{41}$$

Equating all block elements yields the Riccati differential equation and U_{11},

$$\frac{\mathrm{d}R}{\mathrm{d}X} = A_{21} + A_{22}R - RA_{11} - RA_{12}R, \tag{42}$$

$$U_{11} = A_{11} + A_{12}R. \tag{43}$$

Equation (42) can be solved using the shooting method with the LSODE adaptive numerical backward integrator package. To address the numerical stiffness, we use the analytic Jacobian tensor.

$$\frac{\partial\left(\frac{dR}{dX}\right)_{i,j}}{\partial R_{k,l}} = \left(A_{22}\right)_{i,k}\delta_{j,l} - \delta_{i,k}\left(A_{11}\right)^{T}_{j,l} - \delta_{i,k}\left(A_{12}R\right)^{T}_{j,l} - \left(RA_{12}\right)_{i,k}\delta_{j,l}, \tag{44}$$

where $i,k \in \{1,\ldots p\}$, $j,l \in \{1,\ldots q\}$ and $\delta_{i,j} = 1$ if $i = j$ and otherwise 0.

Once equation (42) is solved, equation (38) is transformed to equation (40) and its nontrivial part is

$$\frac{\mathrm{d}w_1}{\mathrm{d}X} = \left(A_{11} + A_{12}R\right)w_1. \tag{45}$$

At the large X limit ($X = X_M$), we can find $w_1(X_M) = y_1(X_M)$ by imposing asymptotic boundary conditions: $(B_1 y_1)_i(X_M) + (B_2 y_2)_i(X_M) = b_i(X_M)$, with $i \in \{1,\ldots q\}$, $B_1(X_M) \in \mathbf{C}^{q,q}$, $B_2(X_M) \in \mathbf{C}^{p,q}$ and $b(X_M) \in \mathbf{C}^{q}$. The matrix representation is

$$\begin{bmatrix} B_1(X_M) & B_2(X_M) \end{bmatrix} \begin{bmatrix} y_1 \\ y_2 \end{bmatrix} = b(X_M). \tag{46}$$

Taking an inverse yield $w_1(X_M)$,

$$w_1(X_M) = \left(B_1(X_M) + B_2(X_M)R(X_M)\right)^{-1} b(X_M). \tag{47}$$

Equation (45) can be solved from X_M to 0 with $w_1(X_M)$. This process is referred to as *backward sweeping*. We make use of the cubic Hermite interpolant to have the Riccati matrix continuous. The analytic Jacobian tensor is

$$\frac{\partial\left(\frac{\mathrm{d}w_1}{\mathrm{d}X}\right)_i}{\partial\left(w_1\right)_j} = \left(A_{11} + A_{12}R\right)_{ij}. \tag{48}$$

Finally full solutions $[y_1, y_2]$ can be recovered using $y_1 = w_1$ and $y_2 = Ry_1$.

Now, let us apply the Riccati transformation method to solve equations (17)–(20) with the parity boundary conditions (equations (24)–(27)) and asymptotic boundary conditions (equations (28)–(31)).

In view of the boundary layer problem, we have already divided the inner and outer layers. Subsequently, we now subdivide the inner layer into left and right regions. It is found that subdivision is helpful for robust usage through trial and error. Left and right regions have different forms of ode systems with defects but are complementary to each other. The two regions will be connected.

We set the field vector in left region Y_l and its corresponding ode system as follows,

$$Y_l(X) = \begin{bmatrix} \tilde{\psi} \\ \dot{\tilde{\phi}} \\ \ddot{\tilde{\phi}} \\ \tilde{\phi} \\ \dot{\tilde{Z}} \\ \tilde{V}_z \\ \dot{\tilde{\psi}} \\ \tilde{\phi} \\ \ddot{\tilde{\phi}} \\ \tilde{Z} \\ \dot{\tilde{V}}_z \end{bmatrix}, \quad y_{l1}(X) = \begin{bmatrix} \tilde{\psi} \\ \dot{\tilde{\phi}} \\ \ddot{\tilde{\phi}} \\ \dot{\tilde{Z}} \\ \tilde{V}_z \end{bmatrix}, \quad y_{l2}(X) = \begin{bmatrix} \dot{\tilde{\psi}} \\ \tilde{\phi} \\ \dot{\tilde{\phi}} \\ \tilde{Z} \\ \dot{\tilde{V}}_z \end{bmatrix}, \tag{49}$$

$$\frac{\mathrm{d}Y_l}{\mathrm{d}X} = A_l Y_l, \tag{50}$$

where matrix coefficients of A_l are given in the appendix, and dots over fields denote derivative and y_{l2} consist of odd fields. Then, $y_{l2}(0) = 0$ is automatically satisfied. However, it is observed that the Riccati matrix blows up during the forward sweeping when D/c_β is high presumably because the maximum power of A_l is 4, a coefficient of X^4 is $(D/c_\beta)^4$, e.g. $A_{l3,7}$. A change of variables is taken to resolve the solution blow-up. We transformed fields ($\tilde{\psi}$, $\tilde{\phi}$, $\dot{\tilde{\phi}}$, $\tilde{Z}$ and $\tilde{V}_z$) to ($\tilde{\psi}$, $\tilde{\delta}$, $\tilde{\xi}$, $\tilde{\eta}$ and $\tilde{V}_z$) and their derivatives too. $\tilde{\delta}$, $\tilde{\xi}$ and $\tilde{\eta}$ are

$$\tilde{\delta} = (Q - Q_{*\mathrm{e}})\tilde{\psi} - X\left(\tilde{\phi} - \tilde{Z}\right) \tag{51}$$

$$\tilde{\xi} = Q\tilde{Z} - Q_{*\mathrm{e}}\tilde{\phi} \tag{52}$$

$$\tilde{\eta} = \ddot{\tilde{\phi}} + \tau\ddot{\tilde{Z}}. \tag{53}$$

Using the transformed variables, we set the field vector in right region Y_r and its corresponding ode system as follows,

$$Y_r(X) = \begin{bmatrix} \tilde{\psi} \\ \tilde{\delta} \\ \dot{\tilde{\xi}} \\ \dot{\tilde{\eta}} \\ \tilde{V}_z \\ \dot{\tilde{\psi}} \\ \dot{\tilde{\delta}} \\ \tilde{\xi} \\ \tilde{\eta} \\ \dot{\tilde{V}}_z \end{bmatrix}, \quad y_{r1}(X) = \begin{bmatrix} \tilde{\psi} \\ \tilde{\delta} \\ \dot{\tilde{\xi}} \\ \dot{\tilde{\eta}} \\ \tilde{V}_z \end{bmatrix}, \quad y_{r2}(X) = \begin{bmatrix} \dot{\tilde{\psi}} \\ \dot{\tilde{\delta}} \\ \tilde{\xi} \\ \tilde{\eta} \\ \dot{\tilde{V}}_z, \end{bmatrix} \tag{54}$$

$$\frac{\mathrm{d}Y_r}{\mathrm{d}X} = A_r Y_r, \tag{55}$$

where coefficients of A_r are given in the appendix. In this case, the maximum power of A_r becomes 2 and hence the numerical stability during the forward sweeping process is enhanced. However, the parity boundary conditions cannot be imposed at $X = 0$ due to singular A_r. This weakness can be compensated

by the left region. To connect both regions, it is necessary to transform the Riccati matrix for the forward sweeping to the left region to convey the initial condition of the Riccati matrix to the right region. Consider transformation matrix T, satisfying

$$Y_l = T(X)\, Y_r, \quad T = \begin{bmatrix} T_{11}(x) & T_{12}(x) \\ T_{21}(x) & T_{22}(x) \end{bmatrix} \tag{56}$$

where T_{11}, T_{12}, T_{21} and $T_{22} \in \mathbf{C}^{5,5}$ and matrix coefficients are given in the appendix.

In the region on the left, $w_{l2} = 0$ has been already met. To make use of equation (45) in the right region, we enforce $w_{r2} = 0$. Then, the Riccati matrix in the left and right regions, R_l and R_r, are:

$$y_{l2} = R_l y_{l1}, \tag{57}$$

$$y_{r2} = R_r y_{r1}. \tag{58}$$

Equations (56)–(58) represent R_r with R_l, T_{11}, T_{12}, T_{21} and T_{22}.

$$R_r = \left(R_l T_{12} - T_{22}\right)^{-1} \left(T_{21} - R_l T_{11}\right). \tag{59}$$

The left and right regions are connected through equation (59), which facilitates the forward sweeping in the right region. At the large X limit, the asymptotic boundary conditions should be represented by Y_r. After normalizing four fields by $\Psi\Delta_{\rm in}/2$, i.e. artificially putting $\Psi = 2/\Delta_{\rm in}$, asymptotic behaviors are given by

$$\dot{\tilde{\psi}} \to 1 + O\left(\frac{1}{X^2}\right), \tag{60}$$

$$\tilde{\delta} \to O\left(\frac{1}{X}\right), \tag{61}$$

$$\dot{\tilde{\delta}} \to O\left(\frac{1}{X^2}\right), \tag{62}$$

$$\tilde{\xi} \to O\left(\frac{1}{X^2}\right), \tag{63}$$

$$\tilde{V}_z \to O\left(\frac{1}{X^2}\right). \tag{64}$$

The asymptotic boundary conditions are imposed by equation (47), B_{r1}, B_{r2} and b_r.

$$B_{r1} = \begin{bmatrix} 0 & 0 & 0 & 0 & 0 \\ 0 & 1 & 0 & 0 & 0 \\ 0 & 0 & 0 & 0 & 0 \\ 0 & 0 & 0 & 0 & 0 \\ 0 & 0 & 0 & 0 & 1 \end{bmatrix}, B_{r2} = \begin{bmatrix} 1 & 0 & 0 & 0 & 0 \\ 0 & 0 & 0 & 0 & 0 \\ 0 & 1 & 0 & 0 & 0 \\ 0 & 0 & 1 & 0 & 0 \\ 0 & 0 & 0 & 0 & 0 \end{bmatrix},$$

$$b_r = \begin{bmatrix} 1 \\ 0 \\ 0 \\ 0 \\ 0 \end{bmatrix}. \tag{65}$$

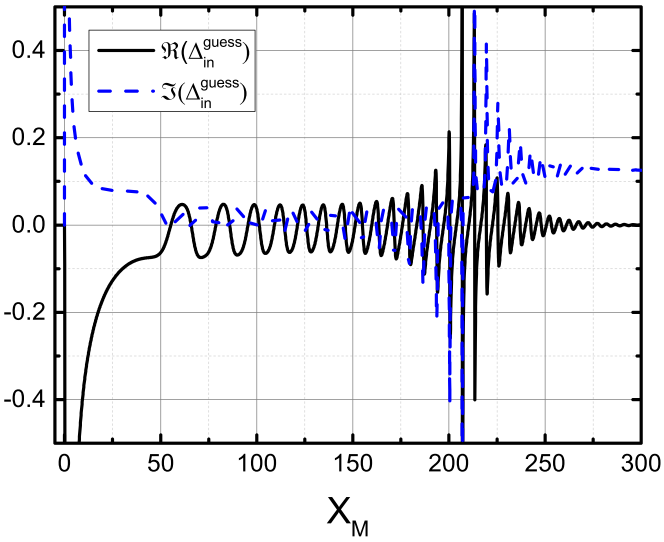

Figure 1. Convergence of $\Delta_{\rm in}^{\rm guess}(X_M)$ despite strong oscillation induced by the kinetic alfven wave due to large D, where $Q = 23$, $Q_e = 2$, $Q_i = -2.6$, $P = 0.5$, $D = 6$ and $c_\beta = 0.7$.

Let the appropriate large X, X_M, above which four fields follow the asymptotic behavior correctly. The suitability of X_M relies solely on convergence of $\Delta_{\rm in}^{\rm guess}(X_M)$ that we guess at X_M using

$$\Delta_{\rm in}^{\rm guess}(X_M) = \frac{2}{\tilde{\psi} - X_M}, \tag{66}$$

since other fields be 0 except for $\tilde{\psi}$ and $\dot{\tilde{\psi}}$ due to equations (60)–(63). Once the convergence is confirmed, $\Delta_{\rm in}$ is found,

$$\Delta_{\rm in} \approx \Delta_{\rm in}^{\rm guess}(X_M) \text{ if } \Delta_{\rm in}^{\rm guess}(X_M) \approx \Delta_{\rm in}^{\rm guess}(X) \;\forall\, X > X_M. \tag{67}$$

Figure 1 shows how $\Delta_{\rm in}^{\rm guess}$ is being converged as X_M is increasing where the plasma parameters are relevant to DIII-D with increased c_β, where $Q = 23$, $Q_{\rm e} = 2$, $Q_{\rm i} = -2.6$, $P = 0.5$, $D = 6$ and $c_\beta = 0.7$. $\Re(\Delta_{in}^{guess})$ and $\Im(\Delta_{\rm in}^{\rm guess})$ converged despite of oscillation induced by kinetic alfven wave featured as large ion Larmor radius $D/c_\beta \sim 10$.

Our methodology is verified by benchmarking it against SLAYER [18], which solves the layer equations in the phase space neglecting $\tilde{V}_z$. Fair comparison demands avoiding the condition $Q \sim Q_{*\rm e}$ where the parallel flow can play a key role. Figure 2 produces substantial agreement in low β plasmas ($c_\beta = 0.1$), yielding $R^2 \approx 0.999$, even though the configuration and phase spaces solved by each method are completely different. This confirms the appropriateness neglecting $\tilde{V}_z$ in low β plasmas except for the condition $Q \sim Q_{*\rm e}$ as well as the fidelity of the proposed method. However, as expected in high β plasmas ($c_\beta = 1$), two results show the difference yielding $R^2 \approx 0.857$. This suggests that the parallel flow should be accounted for in high β plasmas.

The backward sweeping is optionally carried out only if the full solutions are essential to comprehend the four field dynamics in the resonant layer. In such a case, the solutions are

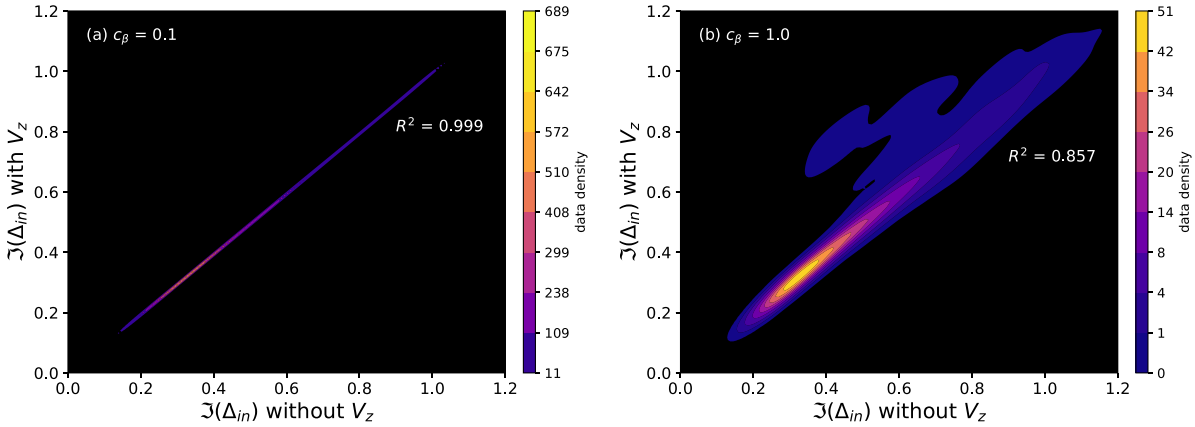

Figure 2. Benchmarking result of $\Im(\Delta_{\rm in})$ with V_z (y axis) against that without V_z (x axis) predicted by SLAYER [18]. The colorbar represents data density from the kernel density estimation. The result is compared between (a) low β case with $c_\beta = 0.1$ and (b) high β case with $c_\beta = 1$. In both cases, D/c_β is 0.1 and 1. Other parameter settings are the same: Q from 1.25 to 10.25 with 1 interval, $Q_{\rm e}$ from 0.5 to 4.0 with 0.5 interval, Q_i from -4.0 to -0.5 with 0.5 interval and P from 0.1 to 100.0 with log-scaled interval 1 while satisfying $Q > Q_{\rm e}$.

reconstructed with the help of an initial condition of $w_{r1}(X_M)$. The entire space is nearly covered by Y_r if the left region is short enough.

4. Resonant layer response in high β plasmas

The parallel flow plays a shielding role in the resonant layer response. Figure 3 displays the effect of parallel flow on $\Im(\Delta_{\rm in})$ and $|\Delta_{\rm in}|$. The red markers take the parallel flow into account. Only the accessible regimes (HRi, HRii, RIii and VRii) are selected near the rotation resonance among the two-fluid drift-MHD regimes, which were mapped out in [16]; the other regimes are inaccessible under the condition $|Q - Q_{*\rm e}| \ll Q$. The chosen parameters are appropriate to represent each regime since the blue markers (numerical outcomes without V_z) correctly follow the black curve (the analytic predictions) in all explored regimes. The higher c_β^2/D^2 is, the more crucial the role of the parallel flow is because the parallel flow accounts for the ion shielding current and the associated $\Delta_{\rm in}^{\rm ion} \propto c_\beta^2/D^2$ as introduced when decomposing $\Delta_{\rm in}$ given by equation (23) in section 2. The parallel flow effect on $\Im(\Delta_{\rm in})$ and $|\Delta_{\rm in}|$ is not outstanding in the HRi and HRii cases due to the low values of $c_\beta/D = 0.1$ (see figures 3(a)–(d)). The parallel flow, however, evidently shifts the zero-crossing condition of Q for $|\Delta_{\rm in}|$ toward the ion diamagnetic rotation direction ($Q_{*\rm i} = -0.15$) due to the higher values of $c_\beta/D \geqslant 1$, as shown in figures 3(e)–(h).

The shifted zero-crossing condition observed in figures 3(g) and (h) suggests that the mode rotation is not locked to the electron rotation. Instead, it shifts to the ion flow direction, of which the mechanism is solely played by the parallel flow response in the absence of NTV [59–63]. Figure 4 shows the parallel flow shielding (ion shielding) by enhancing the mode penetration threshold; the threshold roughly doubles. The shapes of the red curve and blue circular markers are the same in figures 4(a) and (b), i.e. the parallel flow does not change the singular behavior of the magnetic braking force and resonant amplification of $|\Psi|$. However, in the red curve, the parallel flow significantly weakens the magnetic braking force exerted on the resonant layer across $Q \sim Q_{*\rm e}$ since the singular Q decreases to 0.04. The reduced braking force influences the resonant layer response presented in figures 4(c)–(g), where $\Xi(t)$ ramps up linearly in time (see figure 4(c)). The small $|\Psi|$ (figure 4(g)) owing to the mode stabilization confirms that the quasi-linear treatment is appropriate before the mode penetration onset. Once the magnetic braking force is uncompensatable by the restoring viscous force, Q drops such that $\Im(\Delta_{\rm in}) \approx 0$ (see figures 4(d) and (f)) and consequently the resulting Ψ abruptly soars (figure 4(g)). The mode penetration occurs later in the red curve due to the reduced braking force that requires a higher value of Ξ to overwhelm the force balance.

The parallel flow also modifies the field penetration threshold $\Xi_{\rm crit}$. Figure 5 shows $\Xi_{\rm crit}$ as a function of Q_0. The cases where Ψ abruptly transits are only represented by the markers. An illustration of the others is replaced by the analytic prediction (solid curve) and the fitted one (dotted curve). The black curve is in good agreement with the blue markers. This guarantees that the quasilinear analysis can be successfully carried out. $\Xi_{\rm crit}$ has the V-shape with the minimum nearby the zero-crossing rotation for $\Delta_{\rm in}$ because the viscous force is too weak compared to the magnetic braking force if Q_0 is close to the locked Q. The parallel flow completely shifts $\Xi_{\rm crit}$ and plays a shielding role in the field penetration by enhancing $\Xi_{\rm crit}$ at Q_0 above 0.1. Note that the minimum $\Xi_{\rm crit}$ is not zero in the presence of parallel flow. These features are potential candidates to elucidate the shifted field penetration threshold and the non-zero minimum value that are experimentally observed in TEXTOR [38, 39].

The full solution in the layer is completely reconstructed in figure 6, which will be used to comprehend the dominant balancing near the rotational resonance condition.

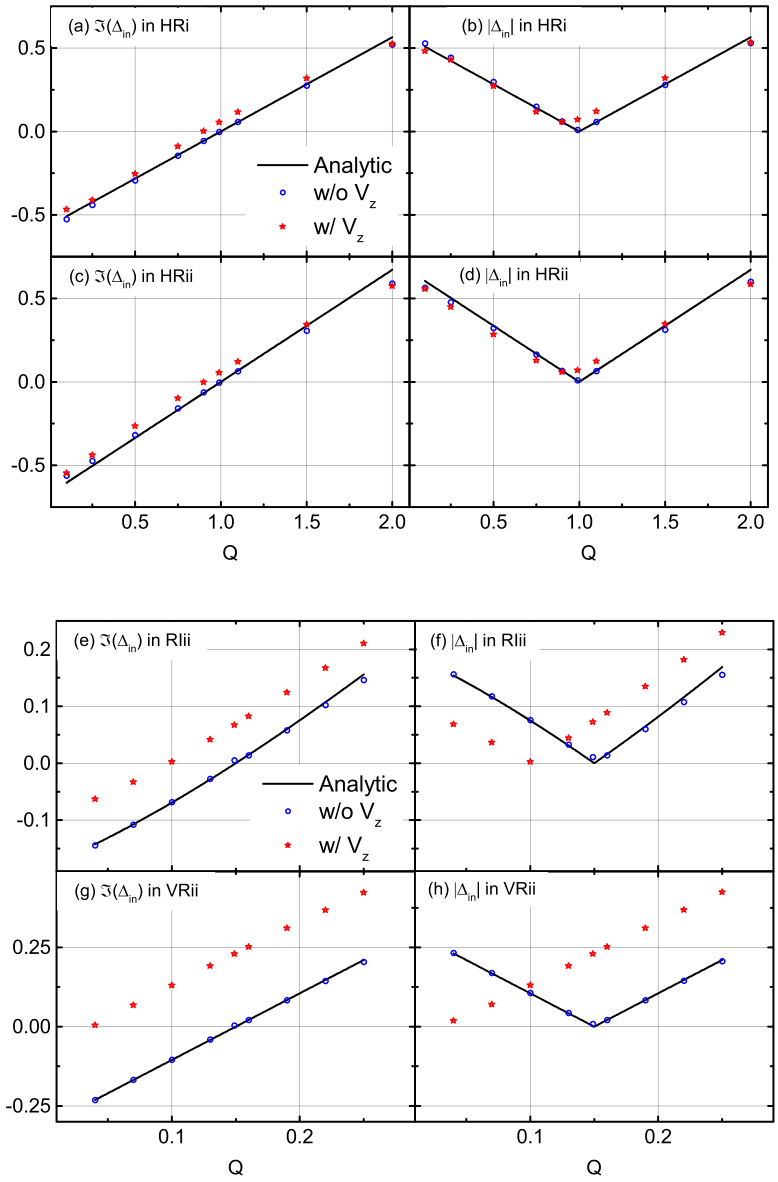

Figure 3. $\Im(\Delta_{\rm in})$ (*a*), (*c*), (*e*), (*g*) and $|\Delta_{\rm in}|$ (*b*), (*d*), (*f*), (*h*) as a function of Q in HRi (*a*), (*b*), HRii (*c*), (*d*), RIii (*e*), (*f*) and VRii (*g*), (*h*) regimes. The red star marker represents a numerical result with V_z, the blue circle marker is a numerical result without V_z (calculated by SLAYER) and the black solid line is an analytic solution [16]. The HRi regime is first Hall resistive regime with $Q_{*\rm e}=1$, $Q_{*\rm i}=-1$, $c_\beta=1$, $D=10$ and $P=1$. The HRii regime is the second Hall resistive regime with $Q_{*\rm e}=1$, $Q_{*\rm i}=-1$, $c_\beta=1$, $D=10$ and $P=0.1$. The RIii regime denotes the second resistive inertial regime with $Q_{*\rm e}=0.15$, $Q_{*\rm i}=-0.15$, $c_\beta=1$, $D=1$ and $P=0.0001$. VRii regime is the second viscous resistive regime with $Q_{*\rm e}=0.15$, $Q_{*\rm i}=-0.15$, $c_\beta=1$, $D=0.1$ and $P=1$.

The proposed method in section 3 successfully solves equations (17)–(20) and hence proves its capability of handling numerical stiffness since the reconstructed fields correctly follow their asymptotic behavior: $\Re(\tilde{\psi})\to\Re(2/\Delta_{\rm in})+|X|$, $\Im(\tilde{\psi})\to\Im(2/\Delta_{\rm in})$, $\Re(\tilde{\phi})\to Q(\Re(2/\Delta_{\rm in})+|X|)/X$, $\Im(\tilde{\phi})\to Q\Im(2/\Delta_{\rm in})/X$, $\Re(\tilde{Z})\to Q_{*\rm e}(\Re(2/\Delta_{\rm in})+|X|)/X$, $\Im(\tilde{Z})\to Q_{*\rm e}\Im(2/\Delta_{\rm in})/X$, $\Re(\tilde{V}_z)\to 0$ and $\Im(\tilde{V}_z)\to 0$ with $\Psi=2/\Delta_{\rm in}$, as written in equations (28)–(31). We also crosscheck that the derivative terms directly reconstructed by the backward sweeping align well with those obtained by numerically discretizing the associated fields. Therefore, the reconstructed solutions are reliable.

Figure 7 shows the balance of terms, evaluated with the reconstructed fields, in equations (17) and (18). The resonance condition $Q\sim Q_{*\rm e}$ inhibits the equilibrium electron flow. According to previous studies neglecting the parallel flow, the magnetic topology should evolve to the fully-reconnected state [3, 4, 15–17, 31]. Nevertheless, in the presence of a parallel flow response, the shielding current giving rise to the magnetic diffusion is sustained by the convective flow of the equilibrium magnetic flux by the perturbed electron flow. Indeed, the dominant balancing in the magnetic equilibrium given by equation (17) is achieved between the blue and red curves, illustrated in figures 7(*a*) and (*b*). The contribution of ions to

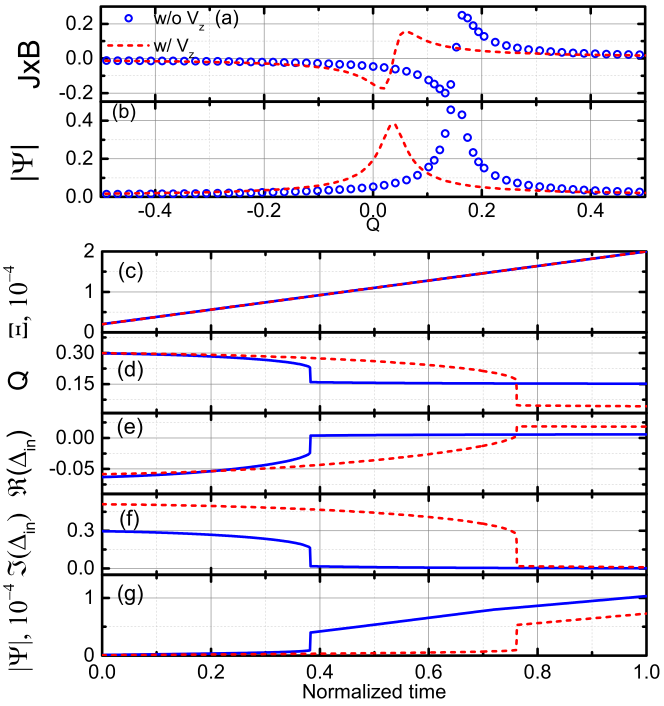

Figure 4. Magnetic braking force, $< \vec{J} \times \vec{B} \cdot \hat{y} >$, (*a*) and $|\Psi|$ (*b*) as a function of Q, respectively, with $\Xi = 1$ as well as Ξ (*c*), Q (*d*), $\Re(\Delta_{\rm in})$ (*e*), $\Im(\Delta_{\rm in})$ (*f*) and $|\Psi|$ (*g*) as a function of the normalized time. Parameters are the same as those of the VRii regime (figures 3(*g*) and (*h*)) while $\varepsilon = 0.01$, $k = 1$ and $Q_0 = 0.3$ are additionally set. Red dashed and blue solid lines (or blue circle markers) indicate with and without V_z, respectively.

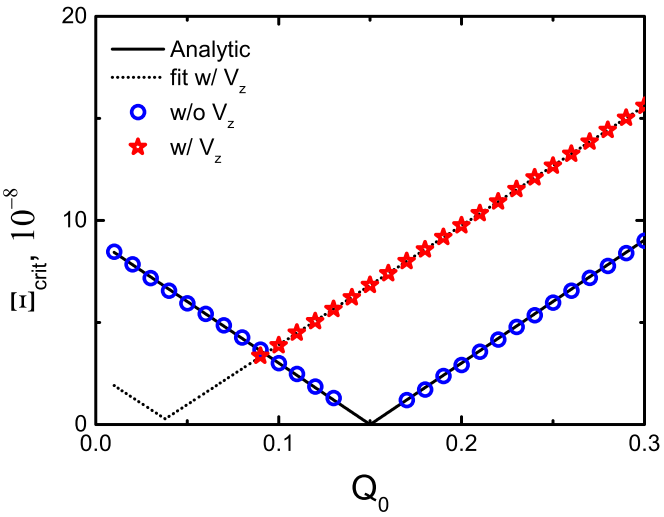

Figure 5. The field penetration threshold as a function of Q_0. Parameters are the same as those of the VRii regime (figures 3(*g*) and (*h*))) with $\varepsilon = 10^{-4}$. The red star marker represents a numerical result with V_z, the blue circle marker is a numerical result without V_z (calculated by SLAYER) and the black solid line is an analytic solution [16]. The dotted line is the fitted result of the red markers.

the shielding current is comparable to that of electrons. As found in figures 7(*c*) and (*d*), the parallel flow term $i c_\beta^2 X \tilde{V}_z$ has the leading order in the dominant balancing of equation (18). Note that the order of $Q\tilde{Z} - Q_{*\rm e}\phi$ is equivalent to that of others in real parts (figure 7(*c*)) and is even negligible in imaginary parts (figure 7(*d*)), as discussed in the $\beta \to \infty$ limit in section 2.

To understand the relationship between β and the parallel flow, it is necessary to relax the $\beta \to \infty$ limit used in the analyses conducted above. Figure 8 shows the β dependence of the magnetic braking force. The three-field model without parallel flow (black curve) represents the $c_\beta \to 0$ limit while keeping other parameters the same, such as D. In this case, the magnetic braking force clearly crosses zero at $Q = Q_{*\rm e}$.

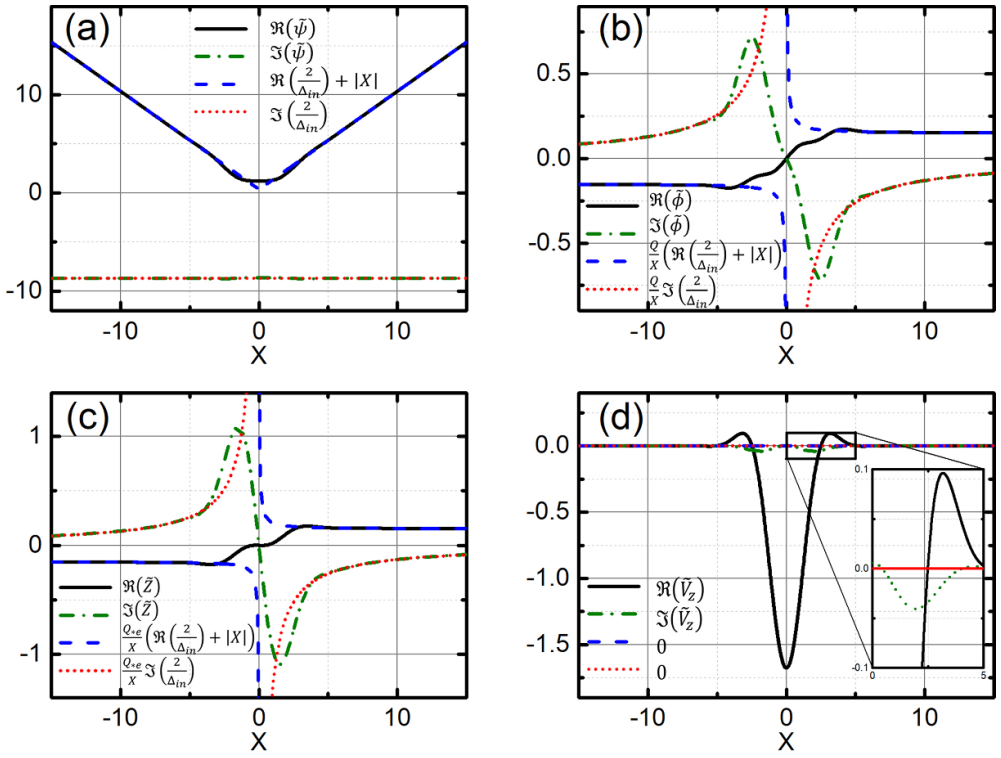

Figure 6. Fully reconstructed four fields ($\tilde{\psi}$ (*a*), $\tilde{\phi}$ (*b*), $\tilde{Z}$ (*c*) and $\tilde{V}_z$ (*d*)) nearby the rotation resonance condition $Q = 0.149 \sim Q_{*e} = 0.15$ (same parameters to those of the VRii regime in figures 3(*g*) and (*h*)). Black solid and green dashed-dotted lines are real and imaginary parts of the four fields, respectively. Blue dashed and red short-dotted lines are real and imaginary parts of large X asymptotes of the four fields, respectively (see equations (28)–(31)). $\Psi = 2/\Delta_{\rm in}$ is used.

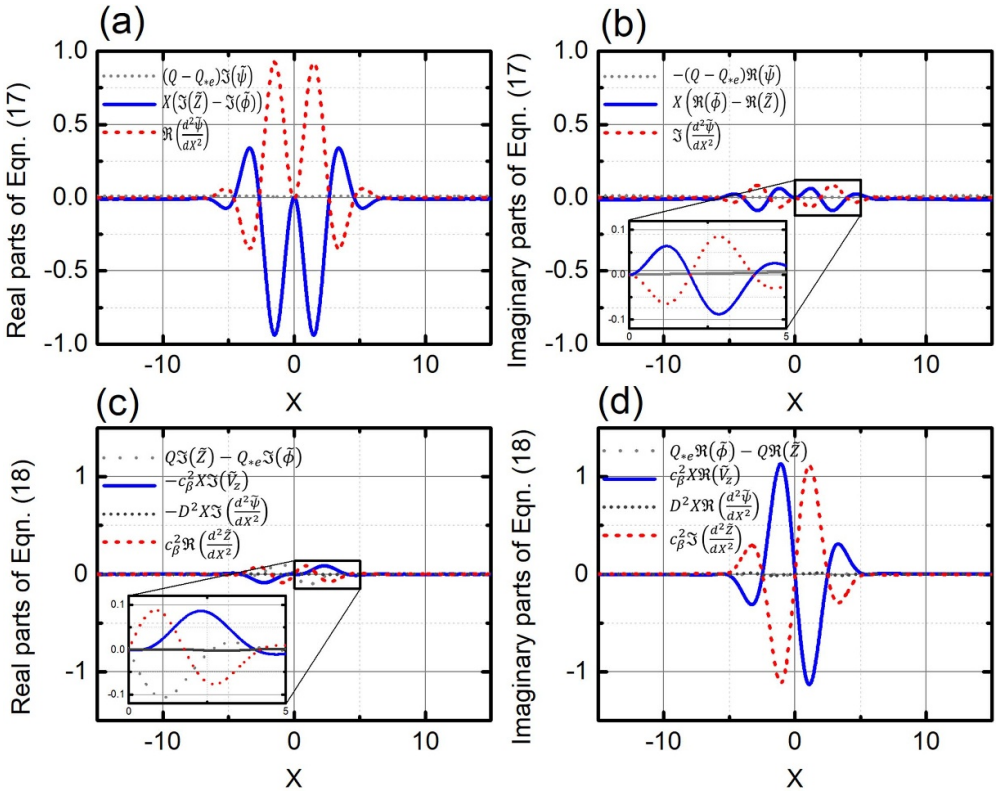

Figure 7. Fully reconstructed balances of equations (17) (*a*), (*b*) and (18) (*c*), (*d*) nearby the rotation resonance condition $Q = 0.149 \sim Q_{*e} = 0.15$ (same parameters to those of the VRii regime in figures 3(*g*), (*h*). (*a*), (*c*) and (*b*), (*d*) show real and imaginary parts, respectively.

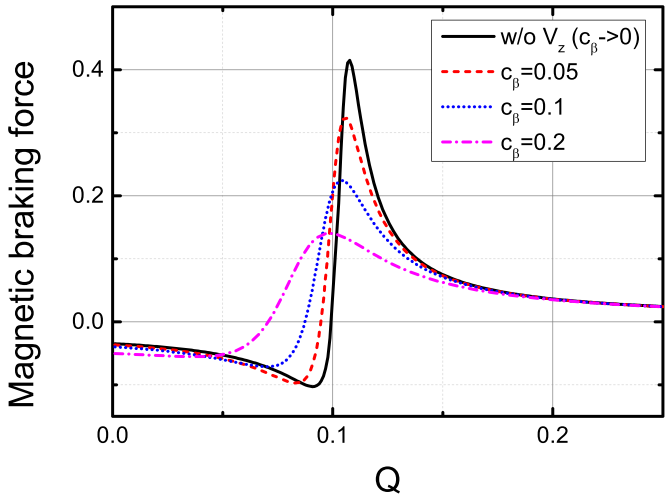

Figure 8. Magnetic braking force as a function of Q. $Q_{*e} = 0.1$, $Q_{*i} = -0.1$, $P = 100$, $D = 0.2\varepsilon = 0.01$ and $k = 1$. The black solid line represents the $c_\beta \to 0$ limit, the red dashed line is $c_\beta = 0.05$, the blue dotted line is $c_\beta = 0.05$ and the magenta dotted-dashed line is $c_\beta = 0.2$.

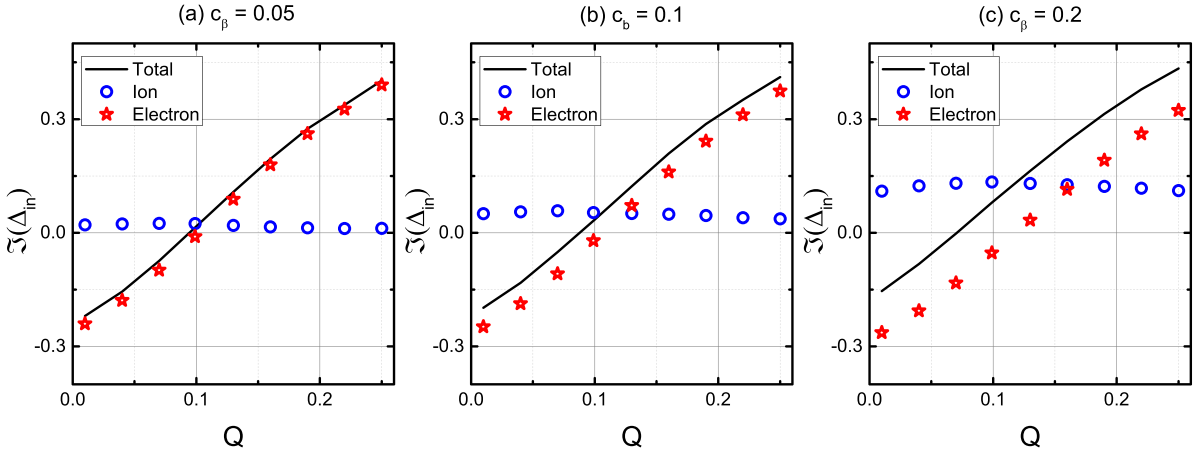

Figure 9. The decomposition of $\Im(\Delta_{\rm in})$ (black line) into $\Im(\Delta_{\rm in}^{\rm ion})$ (blue circle) and $\Im(\Delta_{\rm in}^{\rm electron})$ (red star). $c_\beta = 0.05$ (*a*), 0.1 (*b*) and 0.2 (*c*). Other parameters are the same to those in figure 8.

However, the higher c_β is, the lower zero-crossing Q is. It is worth remarking that the *local* β associated with $c_\beta = 0.2$ is 0.04 and thus accessible enough in the high β tokamak plasmas. For instance, the $Q \sim 5$ ITER steady-state operation scenario (Q is for fusion gain here, not $E \times B$ rotation) has $n_{\rm e} \approx n_{\rm i} = 6 \cdot 10^{19}\,{\rm m}^{-3}$ and $T_{\rm e} \approx T_{\rm i} = 35\,{\rm keV}$ [64]. The resulting (toroidal) $\beta \approx 0.043 > 0.04$ suggests that the parallel flow be of crucial importance in the resonant layer response in future fusion reactors.

The association between the parallel flow and β originates from the dominant balancing of equation (18). For better comprehensibility, the decomposed $\Delta_{\rm in}$ (in equation (23)) is shown in figure 9. When c_β is low, the current carried by ions is much lower than that by electrons, as clarified in figure 9(*a*). However, the ion current contribution becomes critical as c_β increases. Indeed, the mean value of $\Delta_{\rm in}^{\rm ion}$ among the scanned data from $Q = 0.01$ to $Q = 0.25$ with 0.03 intervals (only the $Q = 0.1$ case is replaced as $Q = 0.099$ to avoid singularity) yields 0.018, 0.049 and 0.12 for $c_\beta = 0.05$, 0.1 and 0.2, respectively. This trend is consistent with our expectation on the compressibility. Low β condition implies that the plasmas are easy to compress and the compressibility term has the dominant order in equation (18). As β increases, conversely, the plasmas are difficult to compress and the weakened dominance allows the other terms to play a role.

5. Conclusion

Throughout this work, we report on parallel flow effects in the resonant layer response. After the seminar work on the tearing mode by Furth, Killeen and Rosenbluth [1], Hahm and Kulsrud pioneered the theory of the resonant layer response [3, 4]: resonant perturbations forcing the magnetic flux, which is supposed to be stable, to reconnect. The theory was subsequently elaborated on by Fitzpatrick and Hender [15, 31] who revealed that such mode penetration occurs selectively in the plasma flow. Cole and Fitzpatrick further resolved this

theory using a two-fluid drift-MHD model that includes complex physics. All solutions that were mapped out by them suggest one common point: that the mode is locked to the electron rotation. However, this conclusion is correct only if β is sufficiently low. Otherwise, the locked rotation is shifted due to the parallel flow. The parallel flow influences the layer response by giving rise to the ion shielding current. We elucidate that the higher β is, the more ion current is. As a consequence, in high β plasmas, the parallel flow response not only shifts the zero-crossing condition of Q for $\Delta_{\rm in}$ but also enhances the field penetration threshold (shielding role). Note that the shifting mechanism is purely the outcome of the inner layer response and thus completely distinct from the NTV effect. Incorporation of the parallel flow into $\Delta_{\rm in}$ is the first achievement to our knowledge under the two-fluid drift-MHD formalism.

From a technical point of view, we improve the Riccati transformation method [18] to higher-order ordinary differential systems with asymptotic boundary conditions. The agreement of this method with the original SLAYER demonstrates the fidelity of the proposed method. This development facilitates analysis on more complex systems with asymptotic boundary conditions. The four-field model is implemented in SLAYER, a subroutine of GPEC, and thus is envisaged to design error field corrections and predict the field penetration threshold for high β future fusion reactors. Future work of this study is an extension of the full drift-MHD regimes, where the electron viscosity and thermal conductivity are also retained.

Acknowledgment

This research was supported by National R&D Program through the National Research Foundation of Korea (NRF) funded by the Ministry of Science & ICT (NRF-2019R1A2C1010757). This research was supported by the Brain Pool program funded by the Ministry of Science and ICT through the National Research Foundation of Korea (RS-2023-00284119). This work was supported by the U.S. Department of Energy under Contract Number DEAC02-09CH11466 (Princeton Plasma Physics Laboratory) and by the National Research Foundation of Korea (NRF) grant funded by the Korean government (MSIT) (RS-2024-00350293). The authors also gratefully acknowledge The Research Institute of Energy and Resources and The Institute of Engineering Research at Seoul National University.

Appendix. Matrix coefficients

The only non-zero components of the coefficient matrix of A_l, A_r and T is given here. The matrix coefficients of $A_l(X)$ are

$$A_{l1,6} = 1, \tag{A.1}$$

$$A_{l2,8} = 1, \tag{A.2}$$

$$A_{l3,1} = \frac{Q - Q_{*\rm e} - \tau Q_{*\rm e}}{P} X - i\tau \frac{D^2}{c_\beta^2} (Q - Q_{*\rm e})^2 X - i\tau \frac{Q}{c_\beta^2} \frac{D^2}{c_\beta^2} (Q - Q_{*\rm e}) X - \tau \frac{D^4}{c_\beta^4} (Q - Q_{*\rm e}) X^3, \tag{A.3}$$

$$A_{l3,2} = 4\tau \frac{D^2}{c_\beta^2} X, \tag{A.4}$$

$$A_{l3,4} = -4\tau \frac{D^2}{c_\beta^2} X, \tag{A.5}$$

$$A_{l3,5} = -\tau \frac{Q}{c_\beta^2} X - \tau \frac{Q}{P} X + i\tau \frac{D^2}{c_\beta^2} X^3, \tag{A.6}$$

$$A_{l3,6} = -2\tau \frac{D^2}{c_\beta^2} (Q - Q_{*\rm e}), \tag{A.7}$$

$$A_{l3,7} = -\tau \frac{Q}{c_\beta^2} \frac{Q_{*\rm e}}{c_\beta^2} + 2\tau \frac{D^2}{c_\beta^2} - \frac{X^2}{P} + i\tau \frac{D^2}{c_\beta^2} (Q - Q_{*\rm e}) X^2 + i\tau \frac{Q}{c_\beta^2} \frac{D^2}{c_\beta^2} X^2 + i\tau \frac{D^2}{c_\beta^2} \frac{Q_{*\rm e}}{c_\beta^2} X^2 + \tau \frac{D^4}{c_\beta^4} X^4, \tag{A.8}$$

$$A_{l3,8} = i\frac{Q - Q_{*\rm e}}{P} + i\tau \frac{Q_{*\rm e}}{c_\beta^2} + \tau \frac{D^2}{c_\beta^2} X^2, \tag{A.9}$$

$$A_{l3,9} = \tau \frac{Q^2}{c_\beta^4} - 2\tau \frac{D^2}{c_\beta^2} + \frac{1+\tau}{P} X^2 - i\tau \frac{D^2}{c_\beta^2} (Q - Q_{*\rm e}) X^2 - 2i\tau \frac{Q}{c_\beta^2} \frac{D^2}{c_\beta^2} X^2 - \tau \frac{D^4}{c_\beta^4} X^4, \tag{A.10}$$

$$A_{l3,10} = 2i\tau, \tag{A.11}$$

$$A_{l4,1} = \frac{D^2}{c_\beta^2} (Q - Q_{*\rm e}), \tag{A.12}$$

$$A_{l4,5} = -iX, \tag{A.13}$$

$$A_{l4,7} = -\left(i\frac{Q_{*\rm e}}{c_\beta^2} + \frac{D^2}{c_\beta^2} X^2 \right), \tag{A.14}$$

$$A_{l4,9} = \left(i\frac{Q}{c_\beta^2} + \frac{D^2}{c_\beta^2} X^2 \right), \tag{A.15}$$

$$A_{l6,1} = i(Q - Q_{*\rm e}), \tag{A.16}$$

$$A_{l6,7} = -iX, \tag{A.17}$$

$$A_{l6,9} = iX, \tag{A.18}$$

$$A_{l7,2} = 1, \tag{A.19}$$

$$A_{l8,3} = 1, \tag{A.20}$$

$$A_{l9,4} = 1, \tag{A.21}$$

$$A_{l10,1} = i\frac{Q_{*e}}{P}, \tag{A.22}$$

$$A_{l10,5} = i\frac{Q}{P}, \tag{A.23}$$

$$A_{l10,9} = -i\frac{X}{P}. \tag{A.24}$$

The matrix coefficients of $T(X)$ are

$$T_{1,1} = 1, \tag{A.25}$$

$$T_{2,1} = -\frac{Q}{X^2}, \tag{A.26}$$

$$T_{2,2} = \frac{Q}{Q - Q_{*\rm e}} \frac{1}{X^2}, \tag{A.27}$$

$$T_{2,3} = \frac{1}{Q - Q_{*\rm e}} \tag{A.28}$$

$$T_{2,6} = \frac{Q}{X}, \tag{A.29}$$

$$T_{2,7} = -\frac{Q}{Q-Q_{*\mathrm{e}}}\frac{1}{X}, \tag{A.30}$$

$$T_{3,2} = -\tau\frac{D^2}{c_\beta^2} \tag{A.31}$$

$$T_{3,3} = -i\tau\frac{1}{c_\beta^2}, \tag{A.32}$$

$$T_{3,4} = 1, \tag{A.33}$$

$$T_{3,5} = i\tau, \tag{A.34}$$

$$T_{3,7} = -\tau\frac{D^2}{c_\beta^2}X, \tag{A.35}$$

$$T_{3,10} = i\tau X, \tag{A.36}$$

$$T_{4,1} = -\frac{Q_{*\mathrm{e}}}{X^2} \tag{A.37}$$

$$T_{4,2} = \frac{Q_{*\mathrm{e}}}{Q-Q_{*\mathrm{e}}}\frac{1}{X^2}, \tag{A.38}$$

$$T_{4,3} = \frac{1}{Q-Q_{*\mathrm{e}}}, \tag{A.39}$$

$$T_{4,6} = \frac{Q_{*\mathrm{e}}}{X}, \tag{A.40}$$

$$T_{4,7} = -\frac{Q_{*\mathrm{e}}}{Q-Q_{*\mathrm{e}}}\frac{1}{X}, \tag{A.41}$$

$$T_{5,5} = 1, \tag{A.42}$$

$$T_{6,6} = 1, \tag{A.43}$$

$$T_{7,1} = \frac{Q}{X}, \tag{A.44}$$

$$T_{7,2} = -\frac{Q}{Q-Q_{*\mathrm{e}}}\frac{1}{X}, \tag{A.45}$$

$$T_{7,8} = \frac{1}{Q-Q_{*\mathrm{e}}}, \tag{A.46}$$

$$T_{8,2} = -\tau\frac{D^2}{c_\beta^2}X, \tag{A.47}$$

$$T_{8,8} = -i\tau\frac{1}{c_\beta^2}, \tag{A.48}$$

$$T_{8,9} = 1, \tag{A.49}$$

$$T_{8,10} = i\tau X, \tag{A.50}$$

$$T_{9,1} = \frac{Q_{*\mathrm{e}}}{X}, \tag{A.51}$$

$$T_{9,2} = -\frac{Q_{*\mathrm{e}}}{Q-Q_{*\mathrm{e}}}\frac{1}{X}, \tag{A.52}$$

$$T_{9,8} = \frac{1}{Q-Q_{*\mathrm{e}}}, \tag{A.53}$$

$$T_{10,10} = 1. \tag{A.54}$$

The matrix coefficients of $A_r(X)$ are

$$A_{r1,6} = 1, \tag{A.55}$$

$$A_{r2,7} = 1, \tag{A.56}$$

$$A_{r3,2} = \frac{Q-Q_{*\mathrm{i}}}{c_\beta^2}D^2X, \tag{A.57}$$

$$A_{r3,5} = -i\,(Q-Q_{*\mathrm{i}})X, \tag{A.58}$$

$$A_{r3,8} = i\,\frac{Q-Q_{*\mathrm{i}}}{c_\beta^2}, \tag{A.59}$$

$$A_{r3,9} = -Q_{*\mathrm{e}}, \tag{A.60}$$

$$A_{r4,2} = \frac{1}{P}X - i\,\frac{Q-Q_{*\mathrm{i}}}{P}\frac{D^2}{c_\beta^2}\tau X, \tag{A.61}$$

$$A_{r4,5} = -\frac{Q-Q_{*\mathrm{i}}}{P}\tau X, \tag{A.62}$$

$$A_{r4,8} = \frac{Q-Q_{*\mathrm{i}}}{P}\frac{\tau}{c_\beta^2}, \tag{A.63}$$

$$A_{r4,9} = i\,\frac{Q-Q_{*\mathrm{i}}}{P}, \tag{A.64}$$

$$A_{r5,10} = 1, \tag{A.65}$$

$$A_{r6,2} = i, \tag{A.66}$$

$$A_{r7,1} = 2\frac{Q-Q_{*\mathrm{e}}}{X^2}, \tag{A.67}$$

$$A_{r7,2} = i\,(Q-Q_{*\mathrm{e}}) - \frac{2}{X^2} + \frac{D^2}{c_\beta^2}\,(\tau+1)X^2, \tag{A.68}$$

$$A_{r7,5} = -i\,(\tau+1)X^2, \tag{A.69}$$

$$A_{r7,6} = -2\frac{Q-Q_{*\mathrm{e}}}{X}, \tag{A.70}$$

$$A_{r7,7} = \frac{2}{X}, \tag{A.71}$$

$$A_{r7,8} = i\,(\tau+1)\,\frac{X}{c_\beta^2}, \tag{A.72}$$

$$A_{r7,9} = -X, \tag{A.73}$$

$$A_{r8,3} = 1, \tag{A.74}$$

$$A_{r9,4} = 1, \tag{A.75}$$

$$A_{r10,2} = i\,\frac{Q-Q_{*\mathrm{e}}}{P}, \tag{A.76}$$

$$A_{r10,5} = i\,\frac{Q}{P}, \tag{A.77}$$

$$A_{r10,8} = -i\,\frac{1}{P}\frac{X}{Q-Q_{*\mathrm{e}}}. \tag{A.78}$$

ORCID iDs

Yeongsun Lee https://orcid.org/0000-0003-4474-416X
Jong-Kyu Park https://orcid.org/0000-0003-2419-8667
Yong-Su Na https://orcid.org/0000-0001-7270-3846

References

[1] Furth H.P., Killeen J. and Rosenbluth M.N. 1963 Finite-resistivity instabilities of a sheet pinch *Phys. Fluids* **6** 459–84
[2] Goldston R.J. 2020 *Introduction to Plasma Physics* (CRC Press)
[3] Kulsrud R.M. and Hahm T.S. 1982 Forced magnetic reconnection *Phys. Scr.* **2** 525–8
[4] Hahm T.S. and Kulsrud R.M. 1985 Forced magnetic reconnection *Phys. Fluids* **28** 2412–8
[5] Scoville J.T., La Haye R.J., Kellman A.G., Osborne T.H., Stambaugh R.D., Strait E.J. and Taylor T.S. 1991 Locked

modes in DIII-D and a method for prevention of the low density mode *Nucl. Fusion* **31** 875
[6] La Haye R.J., Fitzpatrick R., Hender T.C., Morris A.W., Scoville J.T. and Todd T.N. 1992 Critical error fields for locked mode instability in tokamaks *Phys. Fluids* B **4** 2098–103
[7] Buttery R.J. *et al* 1999 Error field mode studies on JET, COMPASS-D and DIII-D and implications for ITER *Nucl. Fusion* **39** 1827
[8] Buttery R.J., De'Benedetti M., Hender T.C. and Tubbing B.J.D. 2000 Error field experiments in JET *Nucl. Fusion* **40** 807
[9] Park J.-K., Boozer A.H., Menard J.E. and Schaffer M.J. 2008 Error field correction in ITER *Nucl. Fusion* **48** 045006
[10] Menard J.E. *et al* 2010 Progress in understanding error-field physics in NSTX spherical torus plasmas *Nucl. Fusion* **50** 045008
[11] Park J.-K., Schaffer M.J., La Haye R.J., Scoville T.J. and Menard J.E. 2011 Error field correction in DIII-D ohmic plasmas with either handedness *Nucl. Fusion* **51** 023003
[12] Park J.-K., Menard J.E., Gerhardt S.P., Buttery R.J., Sabbagh S.A., Bell R.E. and LeBlanc B.P. 2012 Sensitivity to error fields in NSTX high β plasmas *Nucl. Fusion* **52** 023004
[13] In Y., Park J.K., Jeon J.M., Kim J. and Okabayashi M. 2015 Extremely low intrinsic non-axisymmetric field in KSTAR and its implications *Nucl. Fusion* **55** 043004
[14] Yang S. *et al* 2024 Tailoring tokamak error fields to control plasma instabilities and transport *Nat. Commun.* **15** 1275
[15] Fitzpatrick R. and Hender T.C. 1991 The interaction of resonant magnetic perturbations with rotating plasmas *Phys. Fluids* B **3** 644–73
[16] Cole A. and Fitzpatrick R. 2006 Drift-magnetohydrodynamical model of error-field penetration in tokamak plasmas *Phys. Plasmas* **13** 032503
[17] Fitzpatrick R. 2022 Influence of anomalous perpendicular transport on linear tearing mode dynamics in tokamak plasmas *Phys. Plasmas* **29** 032507
[18] Park J.-K. 2022 Parametric dependencies of resonant layer responses across linear, two-fluid, drift-MHD regimes *Phys. Plasmas* **29** 072506
[19] Waybright J.C. and Park J.-K. 2024 Effects of electron viscosity on resonant layer responses to non-axisymmetric magnetic perturbations *Phys. Plasmas* **31** 022502
[20] Hazeltine R.D., Kotschenreuther M. and Morrison P.J. 1985 A four-field model for tokamak plasma dynamics *Phys. Fluids* **28** 2466–77
[21] Hazeltine R.D. and Meiss J.D. 2003 *Plasma Confinement* (Courier Corporation)
[22] Fitzpatrick R. and Waelbroeck F.L. 2005 Two-fluid magnetic island dynamics in slab geometry. I. Isolated islands *Phys. Plasmas* **12** 022307
[23] Urquijo G., Bhattacharyya S.N. and Sen A. 1997 Effect of rigid toroidal rotation on the stability of a tokamak plasma to tearing modes *Phys. Plasmas* **4** 239–41
[24] Chandra D., Sen A., Kaw P., Bora M.P. and Kruger S. 2005 Effect of sheared flows on classical and neoclassical tearing modes *Nucl. Fusion* **45** 524
[25] Coelho R. and Lazzaro E. 2007 Effect of sheared equilibrium plasma rotation on the classical tearing mode in a cylindrical geometry *Phys. Plasmas* **14** 012101
[26] Sen A., Chandra D. and Kaw P. 2013 Tearing mode stability in a toroidally flowing plasma *Nucl. Fusion* **53** 053006
[27] Chandra D., Thyagaraja A., Sen A., Ham C.J., Hender T.C., Hastie R.J., Connor J.W., Kaw P. and Mendonca J. 2015 Modelling and analytic studies of sheared flow effects on tearing modes *Nucl. Fusion* **55** 053016
[28] Wang S. and Ma Z.W. 2015 Influence of toroidal rotation on resistive tearing modes in tokamaks *Phys. Plasmas* **22** 122504
[29] White R.L. and Fitzpatrick R. 2015 Effect of rotation and velocity shear on tearing layer stability in tokamak plasmas *Phys. Plasmas* **22** 102507
[30] Cai H., Cao J. and Li D. 2017 Influence of toroidal rotation on tearing modes *Nucl. Fusion* **57** 056006
[31] Fitzpatrick R. 1993 Interaction of tearing modes with external structures in cylindrical geometry (plasma) *Nucl. Fusion* **33** 1049
[32] Park J.-K.Y.U., Boozer A.H. and Glasser A.H. 2007 Computation of three-dimensional tokamak and spherical torus equilibria *Phys. Plasmas* **14** 052110
[33] Hu Q., Logan N.C., Park J.-K., Paz-Soldan C., Nazikian R. and Yu Q. 2020 Nonlinear modeling of the scaling law for the error field penetration threshold *Nucl. Fusion* **60** 076006
[34] Fishpool G.M. and Haynes P.S. 1994 Field error instabilities in JET *Nucl. Fusion* **34** 109
[35] Wolfe S.M. *et al* 2005 Nonaxisymmetric field effects on Alcator C-Mod *Phys. Plasmas* **12** 056110
[36] Park J.-K.Y.U., Schaffer M.J., Menard J.E. and Boozer A.H. 2007 Control of asymmetric magnetic perturbations in tokamaks *Phys. Rev. Lett.* **99** 195003
[37] Logan N.C. *et al* 2020 Empirical scaling of the n = 2 error field penetration threshold in tokamaks *Nucl. Fusion* **60** 086010
[38] Koslowski H.R. Liang Y., Krämer-Flecken A., Löwenbrück K., Hellermann M.V., Westerhof E., Wolf R.C. and Zimmermann O. (TEXTOR team) 2006 Dependence of the threshold for perturbation field generated m/n = 2/1 tearing modes on the plasma fluid rotation *Nucl. Fusion* **46** L1
[39] De Bock M.F.M., Classen I.G.J., Busch C., Jaspers R.J.E., Koslowski H.R. and Unterberg B. 2008 The interaction between plasma rotation, stochastic fields and tearing mode excitation by external perturbation fields *Nucl. Fusion* **48** 015007
[40] Buttery R.J. *et al* 2012 The limits and challenges of error field correction for ITER *Phys. Plasmas* **19** 056111
[41] Fitzpatrick R. 2023 Error-field penetration thresholds in ohmically heated ITER and SPARC plasmas *Phys. Plasmas* **30** 092512
[42] Kim S. *et al* 2024 Highest fusion performance without harmful edge energy bursts in tokamak *Nat. Commun.* **15** 3990
[43] Bender C.M. and Orszag S.A. 1999 *Advanced Mathematical Methods for Scientists and Engineers I: Asymptotic Methods and Perturbation Theory* vol 1 (Springer)
[44] Dieci L., Osborne M.R. and Russell R.D. 1988 A riccati transformation method for solving linear BVPS. I: theoretical aspects *SIAM J. Numer. Anal.* **25** 1055–73
[45] Dieci L., Osborne M.R. and Russell R.D. 1988 A riccati transformation method for solving linear BVPS. II: computational aspects *SIAM J. Numer. Anal.* **25** 1074–92
[46] Park J.-K. and Logan N.C. 2017 Self-consistent perturbed equilibrium with neoclassical toroidal torque in tokamaks *Phys. Plasmas* **24** 032505
[47] Bachmann C. *et al* 2020 Key design integration issues addressed in the eu demo pre-concept design phase *Fusion Eng. Des.* **156** 111595
[48] Zheng J. *et al* 2022 Recent progress in chinese fusion research based on superconducting tokamak configuration *Innovation* **3** 100269
[49] Seok Kim B., Hong S.-H. and Kim K. 2022 Preliminary assessment of the safety factors in k-demo for fusion compatible regulatory framework *Sci. Rep.* **12** 8276
[50] Deshpande S.P. and Maya P.N. 2023 A staged approach to Indian demo *Nucl. Fusion* **63** 126060

[51] Connor J.W., Cowley S.C., Hastie R.J., Hender T.C., Hood A. and Martin T.J. 1988 Tearing modes in toroidal geometry *Phys. Fluids* **31** 577–90
[52] Cowley S.C. and Hastie R.J. 1988 Electron diamagnetism and toroidal coupling of tearing modes *Phys. Fluids* **31** 426–8
[53] Paz-Soldan C., Lanctot M.J., Logan N.C., Shiraki D., Buttery R.J., Hanson J.M., La Haye R.J., Park J.-K., Solomon W.M. and Strait E.J. 2014 atlThe importance of matched poloidal spectra to error field correction in DIII-D *Phys. Plasmas* **21** 072503
[54] Paz-Soldan C., Logan N.C., Lanctot M.J., Hanson J.M., King J.D., La Haye R.J., Nazikian R., Park J.-K. and Strait E.J. 2015 Decoupled recovery of energy and momentum with correction of n = 2 error fields *Nucl. Fusion* **55** 083012
[55] Lanctot M.J. *et al* 2017 Impact of toroidal and poloidal mode spectra on the control of non-axisymmetric fields in tokamaks *Phys. Plasmas* **24** 056117
[56] Vahala G., Vahala L., Harris J.H., Bateman G., Waddell B.V., Dunlap J.L., Paré V.K. and Burris R.D. 1980 Perturbed magnetic-field phase slip for tokamaks *Nucl. Fusion* **20** 17
[57] Craig D., Tan E.H., Schott B., Anderson J.K., Boguski J., Den Hartog D.J., Nishizawa T., Nornberg M.D. and Xing Z.A. 2019 Intrinsic flow and tearing mode rotation in the RFP during improved confinement *Phys. Plasmas* **26** 072503
[58] Huang W. and Zhu P. 2020 Analytical model of plasma response to external magnetic perturbation in absence of no-slip condition *Phys. Plasmas* **27** 022514
[59] Shaing K.-C. and Callen J.D. 1983 Neoclassical flows and transport in nonaxisymmetric toroidal plasmas *Phys. Fluids* **26** 3315–26
[60] Shaing K.-C. 2003 Magnetohydrodynamic-activity-induced toroidal momentum dissipation in collisionless regimes in tokamaks *Phys. Plasmas* **10** 1443–8
[61] Cole A.J., Hegna C.C. and Callen J.D. 2007 Effect of neoclassical toroidal viscosity on error-field penetration thresholds in tokamak plasmas *Phys. Rev. Lett.* **99** 065001
[62] Shaing K.-C., Cahyna P., Becoulet M., Park J.-K., Sabbagh S.A. and Chu M.S. 2008 Collisional boundary layer analysis for neoclassical toroidal plasma viscosity in tokamaks *Phys. Plasmas* **15** 082506
[63] Cole A.J., Hegna C.C. and Callen J.D. 2008 Neoclassical toroidal viscosity and error-field penetration in tokamaks *Phys. Plasmas* **15** 082506
[64] Kim S.H., Polevoi A.R., Loarte A., Yu Medvedev S. and Huijsmans G.T.A. 2021 A study of the heating and current drive options and confinement requirements to access steady-state plasmas at Q 5 in ITER and associated operational scenario development *Nucl. Fusion* **61** 076004